

## Article

# Experimental Investigation and Numerical Simulation of the Fluidity of A356 Aluminum Alloy

Hyeon-Sik Bang<sup>1</sup>, Hyeok-In Kwon<sup>2</sup>, Sung-Bean Chung<sup>3</sup>, Dae-Up Kim<sup>3</sup> and Min-Su Kim<sup>3,\*</sup> 

<sup>1</sup> Advanced Structural Materials R&D Center, Materials Technology R&D Division, Korea Automotive Technology Institute, Cheonan 31214, Republic of Korea

<sup>2</sup> Jeollanam-do Environmental Industries Promotion Institute, Gangjin-gun 59205, Republic of Korea

<sup>3</sup> Jeonbuk Regional Division, Korea Institute of Industrial Technology, Jeonju 54853, Republic of Korea

\* Correspondence: mskim85@kitech.re.kr

**Abstract:** The fluidity of A356 aluminum alloy was experimentally determined at the melt temperatures and vacuum degrees by a series of suction fluidity tests. In order to achieve different cooling rates during the test, quartz tubes, as well as stainless steel tubes, were employed as the fluidity channels. As the melt temperature increased from 650 to 730 °C, fluidity lengths either linearly increased from 26 to 36 cm or parabolically increased from 13 to 29 cm when quartz tubes or stainless steel tubes were employed, respectively. As the vacuum degree of the fluidity test increased from 0.005 to 0.03 MPa, fluidity increased from 25 to 43 cm in quartz tubes while the smaller increase in fluidity from 20 to 31 cm was observed in stainless steel tubes. Shorter fluidity lengths in stainless steel tubes than those in quartz tubes under the same fluidity measurement condition were due to faster solidification speed confirmed by microstructural analysis. In order to predict the fluidity of the A356 alloy obtained from the suction fluidity tests, a mathematical model was developed based on heat and mass transfer equations coupled with thermodynamic calculations by ChemApp software. The simulation results show good agreement with the fluidity length obtained in the present study. From a series of model calculations, the effects of casting parameters on the fluidity of the A356 melt were discussed.

**Keywords:** A356 aluminum alloy; fluidity; suction fluidity test; solidification; fluidity modeling



**Citation:** Bang, H.-S.; Kwon, H.-I.; Chung, S.-B.; Kim, D.-U.; Kim, M.-S. Experimental Investigation and Numerical Simulation of the Fluidity of A356 Aluminum Alloy. *Metals* **2022**, *12*, 1986. <https://doi.org/10.3390/met12111986>

Academic Editor: Ruslan R. Balokhonov

Received: 5 October 2022

Accepted: 17 November 2022

Published: 20 November 2022

**Publisher's Note:** MDPI stays neutral with regard to jurisdictional claims in published maps and institutional affiliations.



**Copyright:** © 2022 by the authors. Licensee MDPI, Basel, Switzerland. This article is an open access article distributed under the terms and conditions of the Creative Commons Attribution (CC BY) license (<https://creativecommons.org/licenses/by/4.0/>).

## 1. Introduction

Recently, Al alloys have been widely used in the automotive industry in order to counteract several critical issues such as weight reduction of vehicles, increasing demand for the electric powertrain system, integration of many parts by single piece casting, etc. In this circumstance, a lot of efforts have been made to develop novel aluminum alloys with excellent mechanical properties or thermal properties. In addition to those excellent properties, the castability of the Al alloys should be considered in the alloy design, especially for large-size thin-walled aluminum die casting.

Generally, the castability of casting alloys was determined by fluidity, which is defined as the distance a liquid metal flows in a mold until it is stopped by solidification. Fluidity is not a physical property, such as density, but a complicated behavior related to the fluid flow and solidification of the liquid or liquid–solid two-phase of an alloy under specific conditions of a casting practice. Therefore, fluidity can be affected not only by the thermodynamic characteristics of the alloy (alloy chemistry [1–9], melt temperature [7,10,11], and viscosity [12,13], etc.) but by various parameters of fluidity tests (measurement method [1,14], mold temperature [15,16], mold coating [17,18], etc.). For example, different fluidity lengths of the A356 alloy from the spiral mold test at the same pouring temperature were reported in the literature studies [14,17]. Due to this complex character of fluidity, direct comparisons and utilization of fluidity data from the literature studies are difficult for the optimization of casting parameters unless the casting conditions are similar to the fluidity measurement conditions.

Therefore, the prediction of the fluidity of an aluminum alloy during the casting process in an arbitrary condition may be useful to find a casting condition with better castability or to develop a novel cast alloy with excellent fluidity. In terms of alloy design, the thermodynamic properties of an aluminum alloy and their impacts on fluidity should be intensively considered in the fluidity modeling. However, the previous research studies on the fluidity simulation [19–22] paid less attention to changes in the thermodynamic properties of an aluminum alloy during the fluidity measurements.

In this study, an attempt is made to develop a mathematical model coupled with thermodynamic calculations to predict the fluidity of an aluminum alloy under various casting conditions. A356 aluminum alloy, a typical cast alloy for gravity or low-pressure die casting, was selected as a starting material for experimental investigation and numerical modeling of the fluidity of aluminum casting alloys. In order to minimize possible experimental errors from fluidity measurements by inconsistent melt and mold conditions, a suction fluidity test, the most simple technique for fluidity measurement, was employed in the present study.

## 2. Experiments

### 2.1. Suction Fluidity Test

The experimental apparatus and procedure of the present suction fluidity test are shown in Figures 1 and 2, respectively. An electric resistance furnace equipped with SiC crucible was used to melt about 120 kg of A356 aluminum ingot. The same amount of A383 alloy, a high-pressure die casting alloy with excellent fluidity, was also prepared and subjected to the suction fluidity test for comparison. Compositions of the two aluminum alloys employed in the present study were summarized in Table 1. The temperature of the aluminum melt was controlled from 650 to 730 °C which covers typical casting temperatures of the A356 alloy in low-pressure die casting. Once the aluminum ingots were fully melted, the gas bubbling filtration process was conducted for 10 min under 10 L/min of Ar flow rate and 200 RPM of rotor speed conditions to remove dissolved hydrogen in the melt. After the removal of dross on the aluminum melt surface, the suction fluidity tests were conducted by using quartz or SS316 stainless steel tubes in the same dimension (OD 8 × ID 6 × L 600 mm). Once a sampling tube was immersed in the aluminum melt, a small amount of the melt started to flow into the tube by opening the valve at the vacuum chamber. The vacuum degree in the vacuum chamber was controlled in the range of 0.005 to 0.03 MPa. When the suction process was finished, the sampling tube was disassembled from the Tygon® tube line and subjected to air cooling. The suction fluidity of the aluminum melt was evaluated by measuring the length of solidified aluminum specimens in the sampling tubes. At least three fluidity tests were done for a typical measurement condition in order to check the reproducibility of the fluidity data.

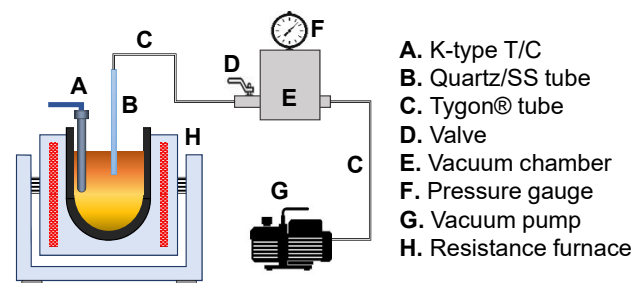


**Figure 1.** Schematic diagram of the experimental apparatus of the present suction fluidity test.

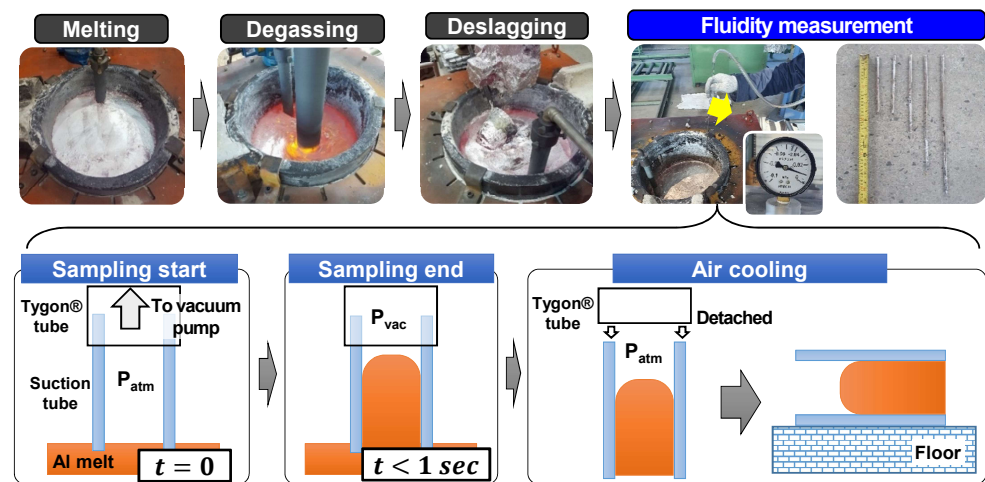


**Figure 2.** The experimental procedure of the present suction fluidity test.

**Table 1.** Alloy compositions (wt%) of the A356 and A383 aluminum alloys employed in the present study.

Alloy	Si	Mg	Mn	Fe	Cu	Ti	Sr	Zn	Al	Liquidus (°C) <sup>†</sup>
A356	7.32	0.35	-	0.10	0.02	0.12	0.014	-	Bal.	618
A383	10.36	0.25	0.19	0.97	1.85	0.04	-	1.17	Bal.	586

<sup>†</sup> Liquidus of each Al alloy was calculated by FactSage [23,24] thermodynamic software and its Al alloy database (FTlite).

## 2.2. Microstructure Observation

The top, middle, and bottom parts of the fluidity samples from the suction fluidity tests were cut, ground, and polished up to 0.04  $\mu\text{m}$  alumina suspension in order to examine the solidification cross-section microstructures of the specimens. The morphology of  $\alpha$ -Al dendrites in the fluidity samples of the A356 alloy was observed by optical microscope (Eclipse MA 200, Nikon, Tokyo, Japan). The dendrite arm spacing of primary  $\alpha$ -Al dendrites was quantitatively measured from optical microscope images by image analysis software (iSolution DT, IMT iSolution Co., Daejeon, Republic of Korea). At least 20 data of dendrite arm spacing were obtained and averaged for accuracy.

## 3. Fluidity Modeling of the A356 Alloy

A schematic diagram to describe the concept of the present fluidity model is shown in Figure 3. At first, all of the model parameters and initial conditions were assigned in the calculation to calculate the initial velocity of the A356 melt at a typical melt temperature and vacuum degree condition. With those initial conditions, model parameters, and initial velocity of the A356 melt, mass transfer of the A356 melt from the furnace to the suction tube was calculated for a time step  $\Delta t$  (0.005 s). Once the length of the A356 melt sucked into the tube for a time step was calculated by solving mass transfer equations, the heat loss of the A356 melt in the tube was calculated by a number of heat transfer equations. This calculation process, mass transfer calculation, and subsequent heat transfer calculation at the same time step was repeated until the velocity of the A356 melts becomes less than 0.001 m/s.

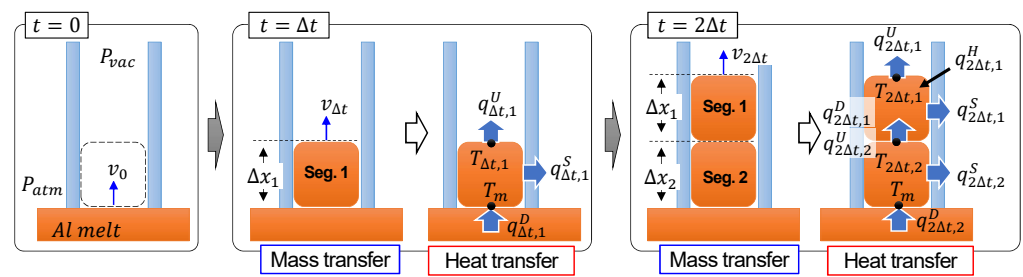


**Figure 3.** Schematic diagram of the calculation process of the present fluidity model.

### 3.1. Mass Transfer Calculation

Similar to the other model describing a suction fluidity test [19,20], the mass transfer of the A356 melts into the suction tube during the suction fluidity test was calculated based on Bernoulli’s equation:

$$\frac{v_{ref}^2}{2g} + \frac{P_{ref}}{\rho g} + x_{ref} = \frac{v_t^2}{2g} + \frac{P_t}{\rho g} + x_t + \Delta h_t \tag{1}$$

where  $v$ ,  $P$ ,  $x$ ,  $\rho$ ,  $g$ , and  $\Delta h$  are the velocity of the melt moving into the suction tube, pressure on the melt, fluidity length, density of the melt, gravitational acceleration, and pressure loss in the A356 melt flowing into the suction tube, respectively. Subscript  $ref$  and  $t$  of  $v$ ,  $P$ ,  $x$  denote the velocity, pressure, and suction length at the reference point, and at the elapsed time  $t$  in seconds after the suction test begins, respectively. For the mass transfer calculation based on Equation (1), the A356 melt was assumed to be incompressible and inviscid. By considering the reference point as the free surface of the A356 melt out of the suction tube,  $v_{ref}$  and  $x_{ref}$  are zero and  $P_{ref}$  is equal to the atmospheric pressure. Therefore, Equation (1) changes into:

$$v_t = \sqrt{\frac{P_{atm} - P_t}{\rho g} - x_t - \Delta h_t} = \sqrt{\frac{P_{vac}}{\rho g} - x_t - \Delta h_t} \tag{2}$$

where  $P_{vac}$  is the vacuum degree of the suction fluidity test. If the time step  $\Delta t$  is small enough to assume  $x_t$  and  $\Delta h_t$  are equal to  $x_{t-\Delta t}$  and  $\Delta h_{t-\Delta t}$ , then  $v_t$  could be calculated from the  $x$  and  $\Delta h$  values at the previous time step. Then fluidity length at time  $t$ ,  $x_t$  could be obtained by:

$$x_t = \sum_{k=0}^{t-1} v_k \Delta t \tag{3}$$

In the present suction fluidity model, pressure loss term  $\Delta h$  consists of three contributions:

$$\Delta h_t = \Delta h_t^f + \Delta h_t^e + \Delta h_t^s \tag{4}$$

$\Delta h_t^f$ ,  $\Delta h_t^e$ , and  $\Delta h_t^s$  are head loss due to friction, head loss at the entrance to the suction tube (entrance loss head), and head loss due to surface tension at time  $t$ , respectively.  $\Delta h_t^f$ , the loss of pressure in tube flow due to resistance near the melt-tube interface, is formulated as:

$$\Delta h_t^f = f_t \frac{x_t v_t^2}{2gd} \tag{5}$$

where  $f_t$  and  $d$  correspond to friction factor at time  $t$  and inner diameter of the suction tube, respectively. Among various formulas of  $f$  reported from literature studies, a formula applicable from laminar flow to turbulent flow [25] was considered in the present fluidity model:

$$f_t = \left( \frac{64}{Re_t} \right) \left( 0.75 \ln \frac{Re_t}{5.37} \right)^{2(a-1)b} \left( 0.88 \ln 3.41 \frac{d}{\epsilon} \right)^{2(a-1)(1-b)} \quad (6)$$

$$a = \frac{1}{1 + \left( \frac{Re_t}{2712} \right)^{8.4}} \quad (7)$$

$$b = \frac{1}{1 + \left( \frac{Re_t}{150d/\epsilon_t} \right)^{1.8}} \quad (8)$$

$$Re_t = \frac{\rho v_t d}{\mu_t} \quad (9)$$

where  $Re_t$ ,  $\epsilon_t$ , and  $\mu_t$  indicate Reynolds number, surface roughness, and viscosity of the A356 alloy at time  $t$ , respectively. For simplicity of the present model, the surface roughness  $\epsilon$  was assumed to be a constant value, 1.5 nm. During the suction fluidity test, the viscosity of the A356 melt moving into the suction tube could be increased due to a decrease in the melt temperature or formation of primary  $\alpha$ -Al by solidification. Therefore, the Einstein–Roscoe type equation was employed to predict the viscosity  $\mu$  of the A356 melt in a liquid single phase or with crystalline phases during the suction fluidity test as below:

$$\mu_t = \mu_t^L \left( 1 - \frac{f_t^s}{f^{sc}} \right)^{-n} \quad (10)$$

where  $\mu_t^L$ ,  $f_t^s$ ,  $f^{sc}$ , and  $n$  are the viscosity of the liquid single phase of the A356 alloy at time  $t$ , mass fraction of solid in the A356 melt at time  $t$ , critical solid fraction, and a model constant, respectively. In the present study,  $\mu_t^L$  was calculated based on the viscosity model for the Al-Cu-Mg-Si system suggested by Zhang et al. [26]. When the temperature of the A356 melt in a suction tube becomes lower than the liquidus temperature of the A356 alloy,  $\mu_t^L$  was assumed to be the viscosity of the A356 melt at liquidus temperature. At every time step, the mass fraction of the solid in the A356 melt was calculated from the equilibrium calculation by ChemApp [27] linked into the main program code in C language with FactSage thermodynamic database (FTLite) [23,24]. The critical solid fraction was considered as a model parameter and optimized to be 0.3 in order to obtain the best agreement with the measured fluidity data.  $n$  was set to be 5 as suggested by the similar suction fluidity modeling research with AC4CH alloy [20].

Other contributions to the pressure loss,  $\Delta h_t^e$  and  $\Delta h_t^s$ , are defined as below:

$$\Delta h_t^e = \zeta \frac{v_t^2}{2g} \quad (11)$$

$$\Delta h_t^s = \frac{4\tau_t}{\rho g d} \quad (12)$$

Here,  $\zeta$ , the entrance loss coefficient, was assumed to be 0.8, which is a typical value for the fluid flow condition from a reservoir into a pipe dipping into the reservoir [28]. Moreover,  $\tau_t$ , the surface tension of the A356 melt at time  $t$  was calculated based on the surface tension model in binary Al-Si liquid suggested by Kobatake et al. [29].

### 3.2. Heat Transfer Calculation

Once the velocity and mass of the A356 melt in the suction tube at a certain time step was determined from the mass transfer calculation, then heat transfer of the melt was calculated by considering the heat balance of the A356 melt in the suction tube as below:

$$q_{t,p}^{st} = q_{t,p}^D + q_{t,p}^U + q_{t,p}^S + q_{t,p}^H \quad (13)$$

$q_{t,p}^{st}$ , heat changes in the segment  $p$  of the A356 melt at time  $t$ , is formulated as below:

$$q_{t,p}^{st} = \rho C_{t-\Delta t,p} \frac{\pi d^2}{4} \Delta x_p \frac{T_{t,p} - T_{t-\Delta t,p}}{\Delta t} \quad (14)$$

where  $C_{t-\Delta t,p}$ ,  $T_{t,p}$ , and  $\Delta x_p$  are the heat capacity of the segment  $p$  of the A356 melt at time  $t - \Delta t$ , temperature of the segment  $p$  of the A356 melt at time  $t$ , and the length of the segment  $p$ , respectively. At every time step, the heat capacity of each segment of the A356 melt at an arbitrary temperature condition was determined by ChemApp calculation [27].

$q_{t,p}^D$ , heat transfer between segment  $p$  and  $p + 1$  (conductive heat transfer into segment  $p$ ) of the A356 melt at time  $t$  is formulated as below:

$$q_{t,p}^D = k_{\text{metal}} \frac{\pi d^2}{4} \Delta x_p \frac{T_{t-\Delta t,p+1} - T_{t-\Delta t,p}}{\Delta x_p} \quad (15)$$

where  $k_{\text{metal}}$  corresponds to the thermal conductivity of the A356 alloy, which is set to be 0.151 kW/m<sup>2</sup>·K [30] in the present model. Similarly,  $q_{t,p}^U$ , the heat transfer between segment  $p - 1$  and  $p$  (conductive heat transfer out of segment  $p$ ) of the A356 melt at time  $t$  is formulated as below:

$$q_{t,p}^U = k_{\text{metal}} \frac{\pi d^2}{4} \Delta x_{p-1} \frac{T_{t-\Delta t,p} - T_{t-\Delta t,p-1}}{\Delta x_{p-1}} \quad (16)$$

For segment 1 (the suction front of a fluidity sample, see Figure 3) of the A356 melt,  $q_{t,p}^U$  is defined as heat convection at the melt–air interface of the segment 1 of the A356 melt at time  $t$ :

$$q_{t,1}^U = h_{\text{Air}} \frac{\pi d^2}{4} (T_{t-\Delta t,1} - T_{\text{Air}}) \quad (17)$$

where  $h_{\text{Air}}$  and  $T_{\text{Air}}$  are the convective heat transfer coefficient of the A356 melt–air interface (0.025 kW/m<sup>2</sup>·K [31]) and atmospheric temperature (25 °C), respectively.

$q_{t,p}^S$ , heat transfer of the segment  $p$  of the A356 melt to the suction tube through the melt–tube interface at time  $t$ , is defined as:

$$q_{t,p}^S = h_{\text{Wall}} \pi d \Delta x_p (T_{t-\Delta t,p} - T_{\text{Wall}}) \quad (18)$$

where  $h_{\text{Wall}}$  and  $T_{\text{Wall}}$  are the heat transfer coefficient at the A356 melt–tube interface and the suction tube temperature (25 °C), respectively. In the present study,  $h_{\text{Wall}}$  values were optimized in order to obtain the best agreement with the measured fluidity lengths at different tube material conditions.  $q_{t,p}^H$ , latent heat of the segment  $p$  of the A356 melt at time  $t$ , is defined as:

$$q_{t,p}^H = \rho \frac{\pi d^2}{4} \Delta x_p (H_{t-2\Delta t,p}^{fus} - H_{t-\Delta t,p}^{fus}) \quad (19)$$

where  $H_{t-\Delta t,p}^{fus}$  is the heat of the fusion of the segment  $p$  of the A356 melt at time  $t - \Delta t$ , which was obtained by the enthalpy difference between the hypothetical single liquid phase and equilibrium phase of the liquid–solid mixture at the temperature of the segment  $p$  from ChemApp [27] equilibrium calculations. All the heat transfer equations on the right-hand side of Equation (13) (Equations (15)–(19)) could be solved by using thermal information of each segment of the A356 melt calculated at previous time steps, and the length of the segment  $p$  derived from the mass transfer calculation at the present time step. Therefore, temperatures of each segment of the A356 melt at the present calculation time  $t$  ( $T_{t,p}$ ) could be calculated from Equation (14) substituted into the left-hand side of Equation (13).

## 4. Results and Discussion

### 4.1. Effect of Melt Temperature on the Fluidity of A356 and A383 Alloy

Figure 4 shows the effect of the melt temperature and superheat on the fluidity of the A356 alloy from suction fluidity tests. As the melt temperature increased, the fluidity of the

A356 alloy increased almost linearly. The linear relationship between melt temperature and fluidity was also found in A383 alloy, showing similar slope. Compared to the fluidity of A383 alloy designed for high-pressure die casting, the fluidity of the A356 alloy designed for gravity or low pressure die casting shows lower values. From other fluidity measurements by using spiral sand mold and strip permanent mold [14] or vacuum suction apparatus [10], linear dependency between fluidity lengths of aluminum alloys and melt temperatures was also confirmed, but the slopes were different from each other. When the fluidity lengths of the two alloys were plotted with respect to superheat (Figure 4b), the fluidity lengths of both A356 and A383 alloys showed the same linear relationship between the suction fluidity and superheat of the melts. From the literature, however, remarkable differences in the fluidity lengths for different aluminum alloys with the same superheat (70 °C) were reported from the strip permanent mold test [14]. Therefore, additional efforts are necessary to clarify the simultaneous effects of superheat and fluidity measurement conditions on the fluidity of aluminum alloys.

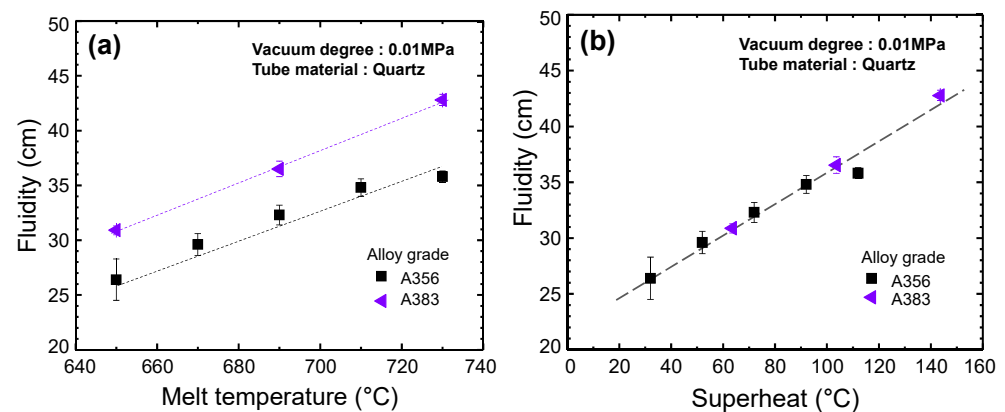


**Figure 4.** The effect of (a) melt temperature and (b) superheat on the fluidity of A356 and A383 alloy.

#### 4.2. Effect of Vacuum Degree on the Fluidity of the A356 Alloy

When the vacuum degree for the suction fluidity tests was increased from 0.005 to 0.03 MPa, fluidity of A356 alloy increased from 25 to 43 cm, as shown in Figure 5a. Unlike the linear dependency between melt temperature and fluidity length, the fluidity of the A356 melt showed a parabolic increase as the vacuum degree increased up to 0.03 MPa. From the point of view of fluid dynamics, the fluidity length should be proportional to the vacuum degree if the pressure loss ( $\Delta h$ ) is negligible in the mass transfer equation (see Equation (1)). However, the friction loss in a tube flow, the major contribution of pressure loss, generally increases as the flow rate increases [28]. Therefore, the gradual increase and convergence of fluidity with an increase of the vacuum degree, as shown in Figure 5a, might be due to higher pressure loss (higher fluidity loss) in the suction flow of the A356 melt under a higher vacuum degree condition.

Figure 5b shows measured fluidity lengths at different melt temperatures under 0.01 and 0.02 MPa of vacuum degree. In terms of the enhancement of the fluidity of the A356 melt, the increase of the vacuum degree was more effective than the increase of melt temperature. For example, fluidity of the A356 melt under 0.01 MPa of vacuum degree was improved from 26 to 33 cm by the melt temperature increase from 650 to 710 °C. A similar degree of fluidity enhancement could be achieved by an increase of the vacuum degree from 0.01 to 0.02 MPa at 650 °C. A linear relationship between suction fluidity and melt temperature with the same slope was observed again when the vacuum degree increased from 0.01 to 0.02 MPa.

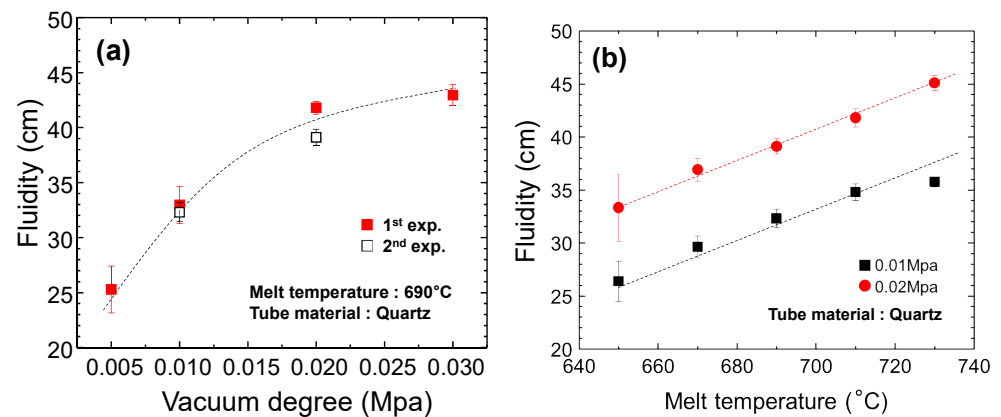


**Figure 5.** The effect of (a) vacuum degree and (b) both vacuum degree and melt temperature on the fluidity of the A356 alloy.

#### 4.3. Effect of Tube Materials on the Fluidity of the A356 Alloy

When the material of suction tubes was changed from quartz to stainless steel, fluidity of the A356 melt decreased by more than 20% as shown in Figure 6a. Especially, the measured fluidity of the A356 melt at 650 °C was drastically decreased when stainless steel suction tubes were employed in the suction fluidity test. As shown in Figure 6b, fluidity lengths measured in stainless steel tubes increased as the vacuum degree increased, but improvement of the fluidity by a higher vacuum degree was less significant in the stainless steel tube when compared to that in the quartz tube. Shorter fluidity lengths of the A356 melt determined in stainless steel tubes might be due to the high solidification rate during the fluidity measurement.

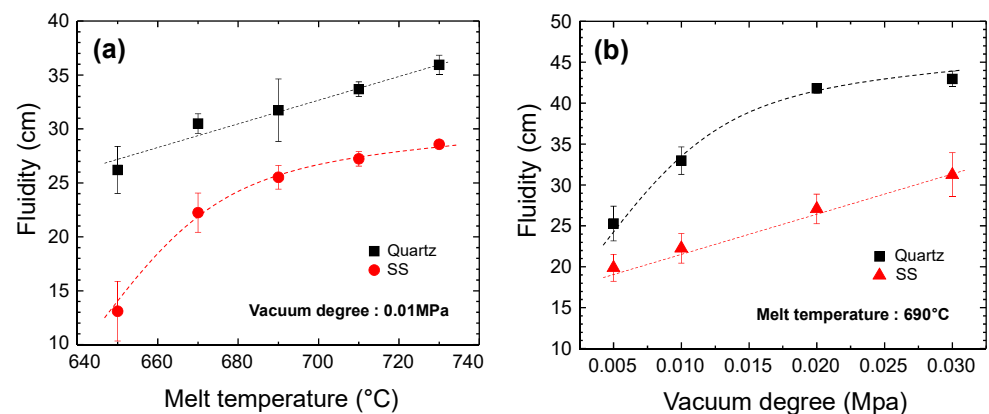


**Figure 6.** The effect of tube materials on the fluidity in the A356 alloy with respect to (a) melt temperature and (b) vacuum degree.

In order to investigate the solidification behavior of the A356 alloy during the suction fluidity measurement, microstructure observation was performed on different positions of fluidity samples measured at 650 °C of the melt temperature and 0.01 MPa of the vacuum degree by both a quartz tube and a stainless steel tube. In the case of the fluidity sample in the quartz tube, the suction front (1-E and 1-C on the left-hand side of Figure 7) has coarse  $\alpha$ -Al dendrites compared to the middle (2-E and 2-C on the left-hand side of Figure 7), and tube entrance (3-E and 3-C on the left-hand side of Figure 7). The slower cooling rate at the suction front could occur due to lower heat transfer from the melt to the air by convection than heat transfer from the melt to the suction tube. Meanwhile, the microstructure of the fluidity sample at the tube entrance (3-E and 3-C on the right-hand side of Figure 7) showed coarser  $\alpha$ -Al dendrites than that at the suction front (1-E and 1-C on the right-hand side of Figure 7) or middle part (2-E and 2-C on the right-hand side of Figure 7) when

a stainless steel tube was employed. Different from a quartz tube, a stainless steel tube absorbed a large amount of heat from the aluminum melt once the tube was immersed into the melt at the beginning of the fluidity measurement. Therefore, the coarse  $\alpha$ -Al dendrites at tube entrance of the fluidity sample from a stainless steel tube can be formed due to low solidification rate by the high temperature of the stainless steel tube. The finer microstructures at the suction front and middle part of the fluidity sample in a stainless steel tube than those in a quartz tube indicates solidification in the A356 melt occurred faster in a stainless steel tube. Regardless of the tube material, the grain size of  $\alpha$ -Al dendrites was bigger at the center of the fluidity sample (1-C, 2-C, 3-C) than at the edge of the sample (1-E, 2-E, 3-E). Size difference of  $\alpha$ -Al dendrites between the center and the edge of the fluidity sample was bigger in the sample from a quartz tube than in the sample from a stainless steel tube, which also suggests a higher solidification rate of the fluidity sample in the stainless steel tube.

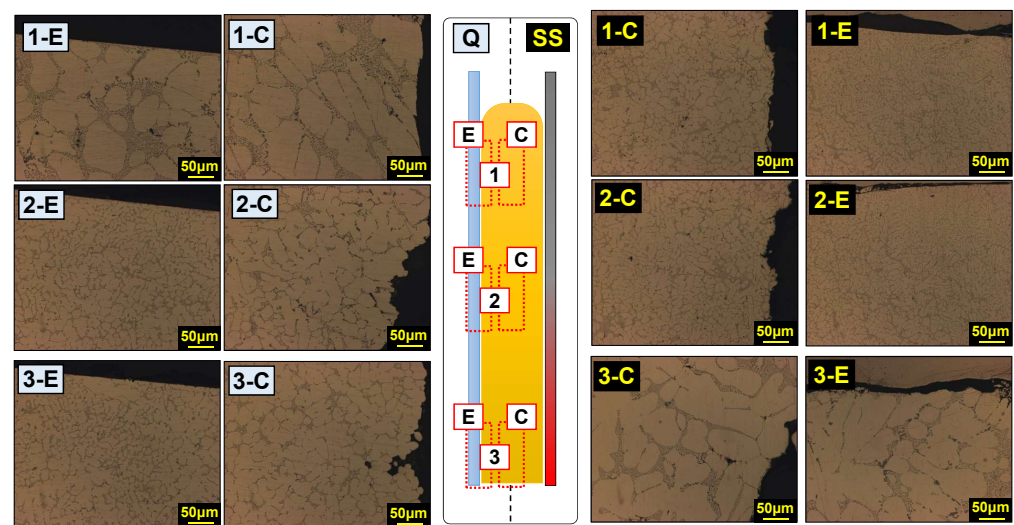


**Figure 7.** Microstructure of the fluidity samples of the A356 alloy obtained at 650 °C of the melt temperature and 0.01 MPa of the vacuum degree in a quartz tube (**left**) and a stainless steel tube (**right**) after air cooling.

In order to estimate the solidification rate of the fluidity samples during the suction fluidity tests, the dendrite arm spacing of  $\alpha$ -Al grains was measured at the different positions. Solidification rates were calculated based on the dendrite arm spacing–cooling rate relationship available from reference [32]. As summarized in Table 2, the solidification rates of the A356 melts in a quartz tube range from 2.15 to 68.2 °C/s. Cooling rates of the A356 melt in a stainless steel tube were predicted to be much higher (maximum 379 °C/s) than those in a quartz tube. If the estimated cooling rates in the fluidity samples were very close to the real solidification rates, solidification of the A356 melt in the stainless steel tube could occur during a very short time (less than a second) of the suction process. Therefore, it was concluded that the fast solidification speed of the A356 melt in a stainless steel tube resulted in short fluidity lengths of the A356 melt in stainless steel tubes.

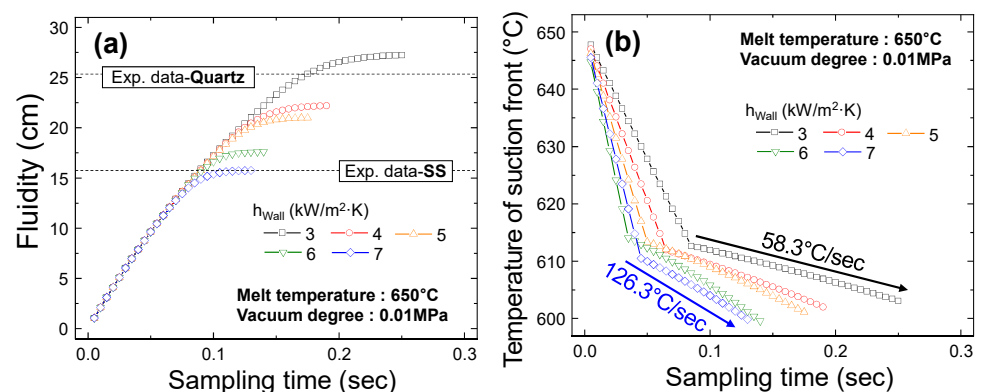
**Table 2.** Dendrite arm spacing and solidification rate of the fluidity samples of the A356 alloy at 650 °C of the melt temperature and 0.01 MPa of the vacuum degree.

Tube Material	Vertical Position	Center		Edge	
		DAS (μm)	Solidification Rate † (°C/s)	DAS (μm)	Solidification Rate † (°C/s)
Quartz	1	32.1	2.15	30.9	2.39
	2	18.1	10.6	10.4	49.6
	3	13.9	21.9	9.29	68.2
Stainless steel	1	7.76	112	5.02	379
	2	8.28	94.0	5.11	359
	3	33.1	1.96	30.7	2.43

† Cooling rate =  $(\text{DAS}/42.328)^{(1/-0.359)}$  [32].

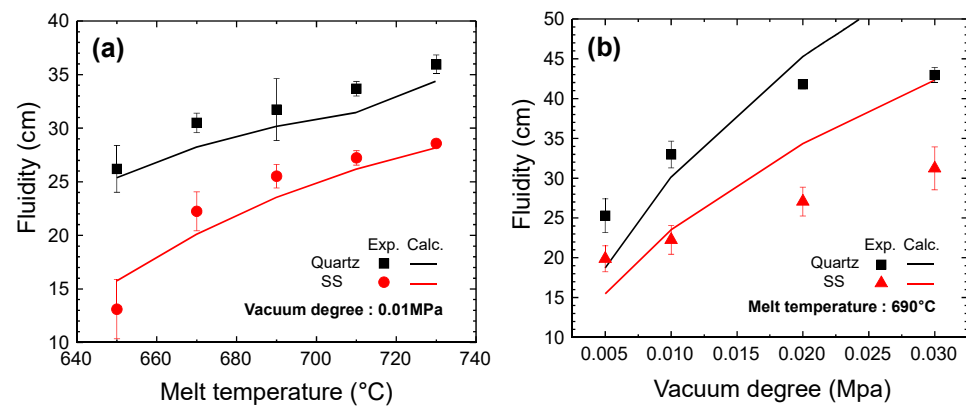
#### 4.4. Calculation Results of the Present Fluidity Model

Figure 8 shows the model calculations of fluidity length and temperature of the suction front at different heat transfer coefficients  $h_{Wall}$  under 0.01 MPa of the vacuum degree and 650 °C of the melt temperature condition. When the  $h_{Wall}$  value increased from 3 to 7 kW/m<sup>2</sup>·K, both fluidity length and sampling time were predicted to decrease (Figure 8a) and the cooling rate was calculated to increase (Figure 8b). The  $h_{Wall}$  values in the best agreement with the measured fluidity lengths (the dotted lines in Figure 8a) were optimized to be 3.8 and 6 kW/m<sup>2</sup>·K for quartz tubes and stainless steel tubes, respectively. According to the calculation results of the present fluidity model, the suction processes of the A356 melts during the fluidity tests were predicted to be finished in less than 0.25 s. The estimated solidification rates of the A356 melts during suction fluidity tests were in the range of 58 to 126 °C/s, which are similar to the calculated cooling rates from the dendrite arm spacing summarized in Table 2. Regardless of the heat transfer coefficient  $h_{Wall}$ , fluid flows in the suction tubes were calculated to be stopped around 605 °C because the solid fraction in the A356 melt calculated by equilibrium calculation became similar to the critical solid fraction at the temperature.

**Figure 8.** Calculation results of the present fluidity model with different heat transfer coefficients: (a) fluidity length and (b) temperature change at the suction front of the fluidity sample.

Calculation results from the present suction fluidity model at 690 °C under different melt temperatures, vacuum degrees, and tube material conditions are shown in Figure 9 with the experimental results. As can be seen from Figure 9a, calculation results of the present suction fluidity model showed good agreement with the measured fluidity data at

different melt temperatures under 0.01 MPa of vacuum degree condition. At the vacuum degree conditions higher than 0.02 MPa, however, the calculated fluidity values showed significant deviations from the experimental data. This discrepancy might come from the simplicity of the present fluidity model or underestimation of friction losses in the model. Within the range of the temperature (650 to 730 °C) and vacuum degree (0.005 to 0.02 MPa) covered in the present study, the fluidity model could be available to optimize the casting parameters for the thin-wall casting of A356 alloy.



**Figure 9.** Comparison of the measured fluidity lengths with the calculation result of the present fluidity model at (a) different melt temperatures, (b) different vacuum degrees.

In order to elucidate the casting parameter which significantly determines the fluidity of the A356 alloy, a series of model calculations were conducted by changing the melt temperature, the vacuum degree, and the heat transfer coefficient  $h_{Wall}$ . Calculated fluidity lengths were summarized in Figure 10 in terms of general casting parameters, such as superheat and initial velocity of the melt. From Figure 10, the most effective casting parameter to enhance the fluidity of the A356 alloy was found to be the initial velocity of the melt regardless of superheat and heat transfer coefficient conditions. Enhancement of fluidity by an increase of superheat was almost negligible at 1.0 or 1.5 m/s of initial velocity condition. At the initial velocity conditions higher than 2.0 m/s, however, fluidity increased remarkably as the superheat increased. Similarly, fluidity lengths at higher initial velocities decreased more remarkably as the heat transfer coefficient from the melt to the mold increased from 3.8 to 5 kW/m<sup>2</sup>·K. Those negligible effects of superheat or heat transfer coefficients on fluidity at low initial velocity conditions could be predicted from the model calculations because the fluid flow of the A356 melt was mainly hindered by friction at the melt channel (or mold) interface, not by viscosity changes with partial solidification in the melt at low fluid velocity conditions. At higher initial velocity conditions, the A356 melt was calculated to travel inside the mold further (longer fluidity length) resulting in a larger interfacial area for heat loss from the melt. In this condition, casting parameters related to the solidification of the A356 melt such as superheat and heat transfer coefficient affect the fluidity remarkably. Nevertheless, the effect of the superheat or heat transfer coefficient on the fluidity of the A356 alloy might be overestimated in the present model due to the low mold temperature (25 °C) set in the model calculation. Even though the application of the present fluidity model is limited to melt superheat, the initial velocity of the melt, and heat transfer coefficient conditions investigated in the present study, the model calculations shown in Figure 10 could be useful to optimize several casting parameters for the thin-wall casting of the A356 alloy with similar casting thickness and to prevent casting failures such as misrun or cold shut.

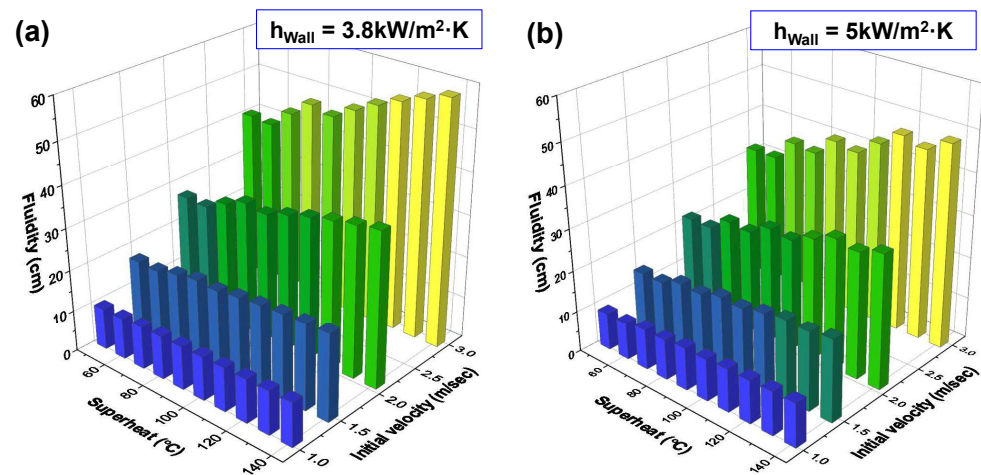


**Figure 10.** Prediction of the fluidity of the A356 melts at arbitrary superheat and initial velocity conditions with different heat transfer coefficients: (a)  $h = 3.8 \text{ kW/m}^2\cdot\text{K}$ , (b)  $h = 5 \text{ kW/m}^2\cdot\text{K}$ .

## 5. Conclusions

The fluidity of the A356 alloy was experimentally investigated at the melt temperatures from 650 to 730 °C and the vacuum degrees from 0.005 to 0.03 MPa by suction fluidity tests with either quartz or stainless steel tubes. As the melt temperature or the vacuum degree of the suction fluidity test increased, the fluidity lengths increased from 25 to 43 cm in quartz tubes while shorter fluidity lengths from 13 to 32 cm were observed in the stainless steel tubes. From the measured dendrite arm spacing of  $\alpha$ -Al grains, the solidification rates in a quartz tube were estimated to be a maximum of 68.2 °C/s; a much faster solidification speed of up to 379 °C/s was determined in a stainless steel tube. By optimizing the heat transfer coefficient parameter, the present suction fluidity model coupled with thermodynamic calculations showed good agreement with the measured fluidity data in both quartz and stainless steel tubes. From a series of model calculations, the initial velocity of the melt was found to be the most effective factor for the improvement of the fluidity of the A356 alloy. Moreover, casting parameters related to solidification, such as superheat and heat transfer coefficients, were found to affect the fluidity more significantly at higher casting speed conditions.

**Author Contributions:** Conceptualization, H.-S.B. and M.-S.K.; methodology, H.-S.B. and M.-S.K.; software, H.-S.B. and M.-S.K.; validation, H.-I.K. and S.-B.C.; formal analysis, H.-I.K.; investigation, H.-S.B., H.-I.K., and S.-B.C.; resources, D.-U.K.; data curation, H.-S.B.; writing—original draft preparation, H.-S.B. and M.-S.K.; writing—review and editing, M.-S.K.; visualization, H.-S.B. and M.-S.K.; supervision, M.-S.K.; funding acquisition, D.-U.K. All authors have read and agreed to the published version of the manuscript.

**Funding:** This research was funded by the Ministry of Trade, Industry, and Energy (MOTIE)/Korea Evaluation Institute of Industrial Technology (KEIT), Rep. of Korea (no. 20010893).

**Institutional Review Board Statement:** Not applicable.

**Informed Consent Statement:** Not applicable.

**Data Availability Statement:** Not applicable.

**Conflicts of Interest:** The authors declare no conflict of interest.

## References

- Shin, J.-S.; Kim, K.-T.; Ko, S.-H.; An, D.-J.; Kim, M.-H. Design and Evaluation of Aluminum Casting Alloys for Thermal Managing Application. *J. Korea Foundry Soc.* **2013**, *33*, 22–31. [[CrossRef](#)]
- Sheshradri, M.R.; Ramachandran, A. Casting fluidity and fluidity of aluminum and its alloys. *Mod. Cast.* **1965**, *21*, 110–122.
- Haga, T.; Imamura, S.; Fuse, H. Fluidity Investigation of Pure Al and Al-Si Alloys. *Materials* **2021**, *14*, 5372. [[CrossRef](#)] [[PubMed](#)]

4. Mollard, F.R.; Flemings, M.C.; Niyama, E.F. Understanding aluminum fluidity: The key to advanced cast products. *AFS Trans.* **1987**, *95*, 647–652.
5. Gowri, S.; Samuel, F.H. Effect of alloying element on the solidification characteristic and microstructure of Al-Si-Cu-Mg-Fe 380 alloy. *Metall. Mater. Trans. A* **1994**, *25*, 437–448. [[CrossRef](#)]
6. Behera, R.; Chatterjee, D.; Sutradhar, G. Effect of reinforcement particles on the fluidity and solidification behavior of the stir cast aluminum. *Am. J. Mater. Sci.* **2012**, *2*, 53–61. [[CrossRef](#)]
7. Adefuye, O.A. Casting fluidity of commercial pure Al-Si casting alloys. *Trans. J. Sci. Technol.* **2014**, *4*, 16–30.
8. Bazhenov, V.E.; Baranov, I.I.; Titov, A.Y.; Sannikov, A.V.; Ozherelkov, D.Y.; Lyskovich, A.A.; Koltygin, A.V.; Belov, V.D. Effect of Ti, Sr, and B Addition on the Fluidity of A356.2 Grade Aluminum Alloy. *Russ. J. Non-Ferr. Met.* **2022**, *63*, 526. [[CrossRef](#)]
9. Zou, G.; Chai, Y.; Shen, Q.; Tengfei, C.; Zhang, H. Analysis of the fluidity and hot tearing susceptibility of AlSi3.5Mg0.5Cu0.4 and A356 aluminum alloys. *Int. J. Metalcast.* **2022**, *16*, 909. [[CrossRef](#)]
10. Timelli, G.; Bonollo, F. Fluidity of aluminium die castings alloy. *Int. J. Cast Met. Res.* **2007**, *20*, 304–311. [[CrossRef](#)]
11. Niesse, J.E.; Flemings, M.C.; Taylor, H.F. Applications of Theory in Understanding Fluidity of Metals. *AFS Trans.* **1959**, *67*, 685–697.
12. Heidazadeh, A.; Emamy, M.; Rhimzadeh, A.; Soufi, R.; Sohrabi Baba Heidary, D.; Nasibi, S. The effect of copper addition on the fluidity and viscosity of an Al-Mg-Si alloy. *J. Mater. Eng. Perform.* **2014**, *23*, 469–476. [[CrossRef](#)]
13. Niu, G.; Mao, J.; Wang, J. Effect of Ce addition on fluidity of casting aluminum alloy A356. *Metall. Mater. Trans. A* **2019**, *50*, 5935–5944. [[CrossRef](#)]
14. Di Sabatino, M.; Arnberg, L.; Apelian, D. Progress on the understanding of fluidity of aluminum foundry alloys. *Int. J. Metalcast.* **2008**, *2*, 17–27. [[CrossRef](#)]
15. Kim, M.-G.; Sung, S.-Y.; Kim, Y.-J. Microstructure, metal mold reaction and fluidity of investment cast-TiAl alloys. *Mater. Trans.* **2004**, *45*, 536–541. [[CrossRef](#)]
16. Brenji, R.V. Effect of reinforcement amount, mold temperature, superheat, and mold thickness on fluidity of in-situ Al-Mg<sub>2</sub>Si composites. *China Foundry* **2018**, *15*, 66–74. [[CrossRef](#)]
17. Tiryakioglu, M.; Askeland, D.R.; Ramsay, C.W. Fluidity of 319 and A356: An Experimental Design Approach. *AFS Trans* **1994**, *102*, 17–25.
18. Pulivarti, S.R.; Birru, A.K. Effect of Mould Coatings and Pouring Temperature on the Fluidity of Different Thin Cross-Sections of A206 Alloy by Sand Casting. *Trans. Indian Inst. Met.* **2018**, *71*, 1735–1745. [[CrossRef](#)]
19. Hiratsuka, S.; Hareyama, T.; Horie, H. Numerical Simulation of Suction Fluidity Test of Flake Graphite Cast Iron. *J. JFS* **2006**, *78*, 675–683.
20. Hiratsuka, S.; Hareyama, T.; Horie, H. Numerical Simulation of Suction Fluidity Test of AC4CH Aluminum Alloy. *J. JFS* **2006**, *78*, 684–690.
21. Bazhenov, V.E.; Petrova, A.V.; Rizhsky, A.A.; Tselovalnik, Y.V.; Sannikov, A.V.; Belov, V.D. Simulation and experimental validation of A356 and AZ91 alloy fluidity in a graphite mold. *Int. J. Metalcast.* **2021**, *15*, 319. [[CrossRef](#)]
22. Di Sabatino, M.; Arnberg, L.; Bonollo, F. Simulation of fluidity in Al-Si alloys. *Metall. Sci. Technol.* **2005**, *23*, 3.
23. Bale, C.W.; Belisle, É.; Chartrand, P.; Degterov, S.; Eriksson, G.; Hack, K.; Jung, I.-H.; Kang, Y.-B.; Melançon, J.; Pelton, A.D.; et al. FactSage thermochemical software and databases - recent developments. *Calphad* **2009**, *33*, 295–311. [[CrossRef](#)]
24. Bale, C.W.; Belisle, É.; Chartrand, P.; Degterov, S.; Eriksson, G.; Gheribi, A.; Hack, K.; Jung, I.-H.; Kang, Y.-B.; Melançon, J.; et al. FactSage thermochemical software and databases, 2010–2016. *Calphad* **2016**, *54*, 35–53. [[CrossRef](#)]
25. Bellos, V.; Nalbantis, I.; Tsakiris, G. Friction Modeling of Flood Flow Simulations. *J. Hydraul. Eng.* **2018**, *144*, 04018073. Erratum in *J. Hydraul. Eng.* **2020**, *146*, 08220005. [[CrossRef](#)]
26. Zhang, F.; Du, Y.; Liu, S.; Jie, W. Modeling of the viscosity in the Al-Cu-Mg-Si system: Database construction. *CALPHAD* **2015**, *49*, 79–86. [[CrossRef](#)]
27. Petersen, S.; Hack, K. The thermochemistry library ChemApp and its applications. *Int. J. Mater. Res* **2007**, *98*, 935–945. [[CrossRef](#)]
28. Munson, B.R.; Young, D.F.; Okiishi, T.H. *Fundamentals of Fluid Mechanics*, 4th ed.; John Wiley & Sons.: New York, USA, 2002; p. 482.
29. Kobatake, H.; Brillo, J.; Schmitz, J.; Pichon, P.-Y. Surface tension of binary Al-Si liquid alloys. *J. Mater. Sci.* **2015**, *50*, 3351–3360. [[CrossRef](#)]
30. Davis, J.R. *ASM Specialty Handbook: Aluminum and Aluminum Alloys*; ASM International: Materials Park, OH, USA, 1993; p. 719.
31. Kosky, P.; Balmer, R.T.; Keat, W.D.; Wise, G. *Exploring Engineering: An Introduction to Engineering and Design*, 5th ed.; Academic Press: Cambridge, MA, USA, 2015; 322p.
32. Spear, R.E.; Gardner, G.R. Dendrite Cell Size. *AFS Trans.* **1963**, *71*, 209.